Temperature and Moisture Impacts on Asphalt before and after Oxidative Aging Using Molecular Dynamics Simulations

Jielin Pan, M.ASCE[1]; Mohammad I. Hossain, A.M.ASCE[2]; and Rafiqul A. Tarefder, M.ASCE[3]

Abstract: Temperature and moisture impacts on unoxidized and oxidized asphalts' thermodynamic and rheological properties were studied using molecular dynamics (MD) simulations. Changes in asphalt property under different degrees of oxidation, temperature, and moisture content were investigated regarding density, isothermal compressibility, bulk modulus, and zero-shear viscosity. MD simulation results show that the density of asphalt before and after oxidation decreases at a similar rate with an increase in temperature. Bulk modulus (inverse of isothermal compressibility) of asphalt before and after oxidation also decreases with an increase in temperature but with different trends. Because of oxidative hardening, oxidized asphalt shows lower isothermal compressibility, but higher bulk modulus and zero-shear viscosity compared with unoxidized asphalt. When moisture is added, such trends become opposite. Specifically, the zero-shear viscosity of the oxidized asphalt becomes lower than that of the unoxidized asphalt above 5% moisture inclusion. This is true in the case of the density of asphalt with moisture as well, but this finding is not significant. **DOI: 10.1061/(ASCE)NM.2153-5477.0000139.**

Author keywords: Asphalt; Oxidation; Computer aided simulation; Thermodynamics; Moisture; Molecular dynamics (MD) simulation; Temperature and moisture; Density; Thermodynamic property; Zero-shear viscosity.

Introduction

The chemical composition of asphalt as an organic pavement material is complex because it contains various types of molecules, from saturated hydrocarbons with no polarity to condensed aromatic ring systems with high polarity (Petersen 1984). Moreover, the underlying chemical composition and chemical properties directly determine the physical properties of asphalt (Greenfield 2011). Asphalt binders serve as an important part of a flexible pavement, and changes in their chemical composition can be ascribable to oxidative aging, variable temperatures, field moisture, etc. These changes often adversely affect the performance and/or durability of flexible pavement (Mannan et al. 2015).

Asphalt concrete durability depends on two major chemical factors: (1) compatibility of intermolecular interactions; and (2) resistance of the chemical composition to reacting with oxygen (Petersen 1984). The latter is called oxidative aging, which causes hardening of asphalt, leads to embrittlement of flexible pavement, and eventually results in excessive pavement cracking (Petersen 2009). Moreover, asphalt is a thermoplastic material. Its physical properties such as density, bulk modulus, viscosity, etc., change with temperature variations. Physical-property changes can be quite significant during asphalt and aggregate mixing, and optimum compaction can also be attributed to rut and crack resistance of asphalt pavements.

Moisture damage is also a major concern for asphalt pavements (Ma et al. 2011; Hossain 2013). Moisture damage is caused by water penetrating into the asphalt-aggregate system and results in rheological property changes of the asphalt binder that shortens the binder's service life and debonds the asphalt from aggregates to accelerate pavement distresses (Chindaprasirt et al. 2009).

This study aims to investigate the impacts of temperature and moisture on asphalt before and after oxidative aging in molecular scale using molecular dynamics (MD) simulation. For many years, oxidative aging resulting from temperature and moisture effects has been investigated separately by mesoscale laboratory tests. For example, Superpave mix design suggests performing moisture-conditioned and unconditioned test by doing indirect tensile tests (IDTs). However, this type of test does not consider combined effects of oxidative aging and moisture-induced damage. Very recently, with the use advanced simulation techniques and sophisticated laboratory equipment such as nanoindentation or atomic force microscopy (AFM), the underlying causes of the combined effects have been investigated. Specifically, MD simulation has been used to understand the molecular-scale behavior of asphalt under different conditions regarding physical, thermodynamic, and rheological behavior before and after oxidative aging. Moreover, MD simulation is very useful for studying how the external properties of asphalt change as a result of internal chemical composition changes under different conditions such as temperature and moisture content.

Several research studies on the properties of asphalt under various conditions have been conducted using MD simulations. Zhang and Greenfield (2007a, b) developed a preliminary asphalt model for virgin/unoxidized asphalt binder and analyzed the properties of unoxidized asphalt model via MD simulations. Their studies included changes of density, thermal expansion coefficient, heat

[1]Engineer I, WSP/Parsons Brinkerhoff, 6100 Uptown Blvd. NE #700, Albuquerque, NM 87110 (corresponding author). E-mail: jlpan@unm.edu; jielin.pan.1@gmail.com

[2]Assistant Professor, Dept. of Civil Engineering and Construction, Bradley Univ., 1501 W Bradley Ave., Peoria, IL 61625. E-mail: mihossain@bradley.edu

[3]Professor, Dept. of Civil Engineering, Univ. of New Mexico, MSC01-1070, Albuquerque, NM 87131-0001. E-mail: tarefder@unm.edu

Note. This manuscript was submitted on December 8, 2015; approved on September 18, 2017; published online on October 23, 2017. Discussion period open until March 23, 2018; separate discussions must be submitted for individual papers. This paper is part of the ***Journal of Nanomechanics and Micromechanics***, © ASCE, ISSN 2153-5434.

capacity, isothermal compressibility, bulk modulus, viscosity, relaxation time, and diffusion under different temperatures. Later, they proposed a new asphalt model to represent the Strategic Highway Research Program (SHRP) AAA-1 asphalt and studied the polymer (polystyrene chain) effects on the microstructure and properties of the asphalt model (Greenfield and Zhang 2009; Zhang and Greenfield 2008, 2010). Subsequently, Li and Greenfield (2014a, b) improved the model asphalt systems for MD simulation including all the four components in asphalt (saturates, aromatics, resins, and asphaltenes) to represent the SHRP AAA-1, AAK-1, and AAM-1 asphalts, which are in good accord with laboratory testing results. They further studied the properties of the revised SHRP AAA-1 asphalt model regarding viscosity change, relaxation time, and dynamics behavior at different temperatures. Martín-Martínez et al. (2015) later modified the asphaltene structures in Li and Greenfield's (2014a, b) asphalt model based on Clar sextet theory to understand better the chemical structures of this class of materials.

Hansen et al. (2013) proposed a united-atom model of asphalt with four components, also called the Cooee-bitumen model, including saturated hydrocarbon, resinous oil, resin, and asphaltene. They characterized the asphalt model regarding dynamical properties, relaxation time, stability of linear asphaltene nanoaggregates, and rheology and molecular structure of the Cooee asphalt model under shear in the non-Newtonian regime using nonequilibrium MD simulations (Lemarchand et al. 2014, 2015). Chemical aging of Cooee asphalt was also investigated by Lemarchand et al. (2013). The oxidative aging reaction was demonstrated by a chemical reaction: 2 resins → 1 asphaltene, and the rheological and dynamical properties of each composition were studied.

Tarefder and Arisa (2011) studied density and energy changes of resin and asphaltene components in asphalt with and without oxygen presence at different temperatures. Pan et al. (2012) studied the potential chemical reactions between asphalt composition and oxygen. The simulations were conducted in an ab initio quantum chemistry–based environment, and X-ray photoelectron spectroscopy (XPS) validated the proposed quantum chemistry–based models.

Nevertheless, none of those mentioned studies analyzed and compared the physical, thermodynamic, and rheological changes of asphalt before and after oxidative aging combined with moisture using MD simulations, which this study does. Specifically, the density response of asphalt to different temperature has not been investigated comprehensively, which is essential for the compaction of asphalt-aggregate mixtures to achieve optimum density during paving construction. Also, the glass transition behavior of asphalt can be interpreted by significant thermodynamic quantity changes of asphalt, such as isothermal compressibility and bulk modulus under certain temperature ranges. Moreover, the moisture effect on asphalt binders before and after oxidation has not been investigated comprehensively. This study compares the density and zero-shear viscosity changes of asphalt before and after oxidative aging at different moisture contents.

Modeling of Asphalt Systems

The largest elements in asphalt are carbon and hydrogen atoms. Heteroatoms such as sulfur, oxygen, nitrogen, etc., can also be found in asphaltic molecules. According to different solubility classes, asphalt can be physically divided through the selective adsorption-desorption method into four fractions (Corbett 1969). As shown in Fig. 1, asphalt possesses a colloidal structure with asphaltene micelles dispersed in maltenes (Lesueur 2009). Except for the asphaltene fraction, maltenes can be separated into additional

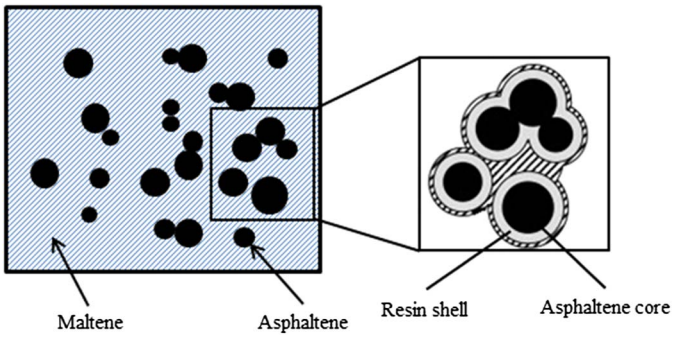

Fig. 1. Schematic diagram of the colloidal structure of asphalt

three fractions: saturates, aromatics, and resins, with an increase in polarity (Lu and Wang 2010; Petersen 1984).

Molecular Structures of Unoxidized Asphalt

This study uses Li and Greenfield's (2014b) improved asphalt system model developed for unoxidized asphalt. Molecular structures were developed according to the four fractions in the asphalt system: saturates, aromatics, resins, and asphaltenes, as shown in Figs. 2(a–d), respectively. However, other asphalt molecular structures are available in the literature (Al Halwachi et al. 2012).

Molecular Structures of Oxidized Asphalt

As organic materials, the properties and chemical reactions of asphalts are determined by their underlying functional groups. With oxygen presence, the sensitive functional groups in asphalt react rapidly with the oxygen and form more polar and strongly interacting chemical functional groups, resulting in increased viscosity and changes in complex flow properties (Petersen 1984).

The oxidized products formed in asphalt are carbonyl compounds (Petersen and Glaser 2011; Petersen 1984). The most sensitive hydrocarbon moiety to oxygen existing in asphalt is benzylic carbon, which is a carbon atom connected to a benzene ring. Ketone is formed at the benzylic carbon by replacing the hydrogen atom attached to it. Another major oxidative reaction is the formation of sulfoxides if any sulfur atoms exist in the molecule. Figs. 3(a and b) illustrate the formation of ketone and sulfoxide during oxidation, respectively (Pan et al. 2012; Petersen 1984).

The molecular structures of asphalt after oxidation were developed according to the existing sensitive functional groups in the unoxidized molecules of aromatic, resin, and asphaltene fractions as shown in Figs. 4(a–c). Because there are no sensitive functional groups in the saturate fraction, the molecular structures of the saturate fraction remained the same after oxidation (Corbett and Merz 1975; Pan et al. 2012; Petersen 1984).

MD Simulation Method

Unoxidized and Oxidized Asphalt Systems Modeling

Before creating a simulation box for asphalt systems, a semiempirical quantum chemistry program *MOPAC* was used for molecular structure optimization to make the proposed molecular structures closer to real molecules in terms of partial charges, missing parameter calculation, and molecular geometry optimization.

An asphalt system before oxidative aging was then created to represent SHRP AAA-1 asphalt binder based on Li and Greenfield (2014b), which is closest to a real asphalt binder when compared to

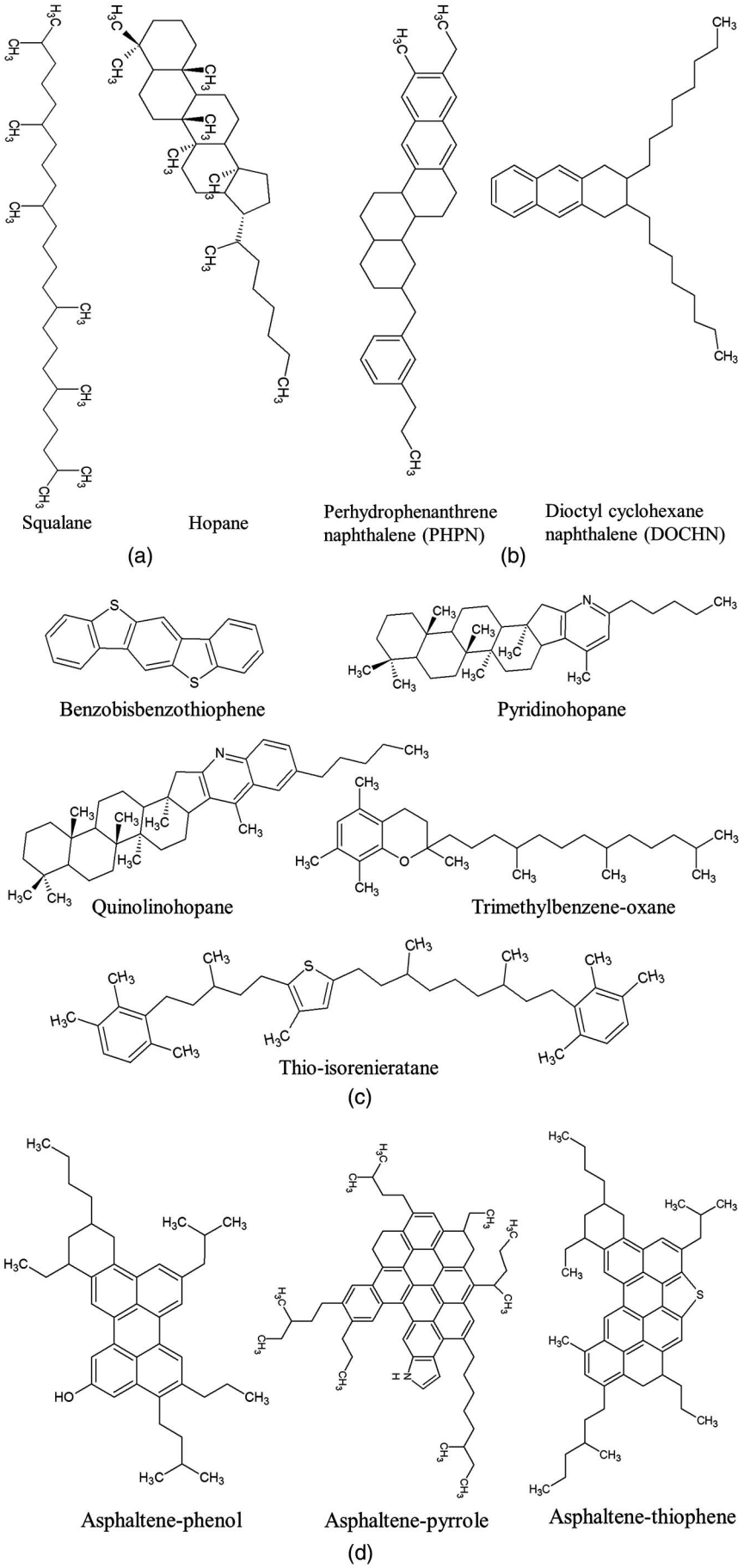

Fig. 2. Molecular structures in asphalt before oxidation: (a) saturates; (b) aromatics; (c) resins; (d) asphaltenes

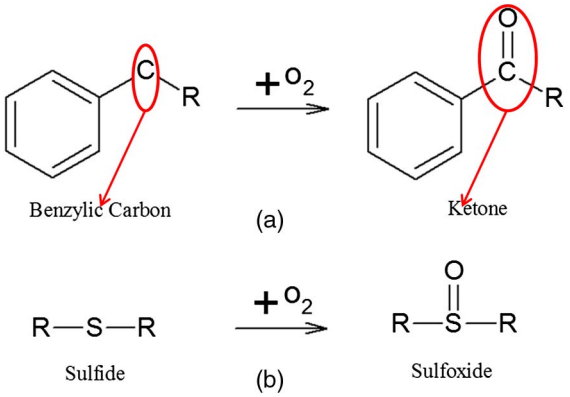

Fig. 3. Reactions with oxygen of most sensitive functional groups in asphalt: (a) formation of ketone; (b) formation of sulfoxide

all the model asphalt systems proposed by Li and Greenfield (2014b). Table 1 lists the composition of the asphalt system before and after oxidation. It is observed that the percentage distributions of the four fractions in the unoxidized asphalt system are in good agreement with experimental data. It also can be seen that after oxidative aging, the percentage of saturate fraction decreases, along with increase percentages of resin and asphaltene fractions. This indicates more polar fractions being formed in the asphalt after oxidation. The initially condensed simulation box size for the model asphalt system was $36 \times 36 \times 36$ Å^3.

All the molecules of unoxidized and oxidized asphalts were put into their individual simulation box to represent an unoxidized asphalt system and oxidized asphalt system, respectively. The size of the simulation box was large enough to contain all the asphalt fractions. Amorphous asphalt systems were then built representing realistic initial conformations of asphaltic molecules. Condensed phases of both unoxidized and oxidized asphalt systems were obtained first, along with energy minimization to remove all nonbonded overlapping between different particles and spread rings by a Monte Carlo minimization algorithm.

The oxidized asphalt system for simulation maintained the same number of molecular structures as the unoxidized asphalt system but was less condensed, with original dimensions of $36.3 \times 36.3 \times 36.3$ Å^3. The creation procedures of both unoxidized and oxidized asphalt systems were the same, and energy minimization was completed for the two asphalt systems to remove nonbonded overlapping.

Periodic boundary conditions were implemented in this study to create the bulk state (gas, liquid, or solid) of asphalt systems before and after oxidative aging. In a periodic boundary-condition model, molecules are initially placed within a simulation box. The molecules not only interact with their neighbors in the same simulation box, but they also interact with images of molecules in neighboring simulation boxes. Thus, during the simulation, a molecule can diffuse to the edge of the simulation box and freely cross over into the next box.

General MD Simulation Parameters

In this study, simulations were conducted in a DREIDING force field under 101.325 kPa (1.0 atm) pressure, which defines the potential intramolecule and intermolecule interactions in the MD simulation systems (Fraaije et al. 2014; Mayo et al. 1990). The smooth particle mesh Ewald (SPME) method was used for handling long-range electrostatic and van der Waals interactions. The temperature and pressure of the systems were controlled by a Berendsen thermostat and barostat, respectively.

To investigate the effects of different cutoff radiuses on simulation results, the simulation time step was set the same for all the simulations. Two cutoff radiuses were considered: 7.5 and 17 Å. The MD simulation systems of both unoxidized and oxidized asphalts were first relaxed using a canonical ensemble that considered number of particles N, volume V, and temperature T (thus also called a NVT ensemble). The simulation time step was set at 0.1 femtosecond (fs) and with simulation duration of 20 picosecond (ps) (200,000 running steps). An isothermal-isobaric ensemble (which considers number of particles N, pressure P, and temperature T to also be called a NPT ensemble) was then used to simulate the realistic asphalt systems and obtain densities of the asphalt systems. The simulation time step under the NPT ensemble was set at 0.5 fs with simulation duration of 500 ps (1 million running steps) to guarantee the system could reach equilibrium.

Fig. 5 shows an equilibrium condition of the MD simulation. Tables 2 and 3 provide numbers of atoms for unoxidized and oxidized asphalt systems. The proportion of each type molecular is fixed. If the system sizes need to be increased for further research, researchers could increase the amount of each atom based on their proportion in the asphalt system and then increase the dimension of the simulation box to accommodate the higher amount of atoms.

Thermodynamic Properties of Unoxidized and Oxidized Asphalt

Simulation Parameters

The simulation systems were first relaxed under a NVT ensemble at −173°C (100.15 K), which maintained the N, V, and T values of the systems as constant. Simulations ran for 20 ps with 200,000 running steps at a time step of 0.1 fs. Then, asphalt systems were simulated under a NPT ensemble, which maintained N, P, and T values of the systems as constant. The ensemble was used to gain densities of the asphalt systems close to those of realistic asphalt under a temperature range of −35 to 160°C (238.15–433.15 K), with a temperature increment of 15°C. This temperature range covers the pavement conditions from cold winter to asphalt-aggregate mixing temperatures. The simulation time step was set at 0.5 fs with 1 million running steps (500 ps). All the unoxidized and oxidized simulation systems were converged after 600,000 running steps in both energy and volume. Pan (2015) has provided examples of the energy and volume changes over the simulation duration for both unoxidized and oxidized asphalts.

Density

Fig. 5 shows one example of the density simulations for unoxidized and oxidized asphalt systems at 25°C. It can be seen that all the density reached equilibrium after 600,000 running steps. This is also the same for all other MD simulations. The average density changes of the unoxidized and oxidized asphalt systems at different temperatures during the last 200,000 equilibrium running steps under the NPT ensemble are shown in Fig. 6. It can be seen the density of both unoxidized and oxidized asphalts decrease with an increase in temperature. Oxidized asphalt has an approximately 60 kg m^{-3} higher density than the unoxidized asphalt at each temperature point. Another observation from the simulations is that compared with the density of unoxidized asphalt, the density of oxidized asphalt decreases slightly more slowly with an increase in temperature.

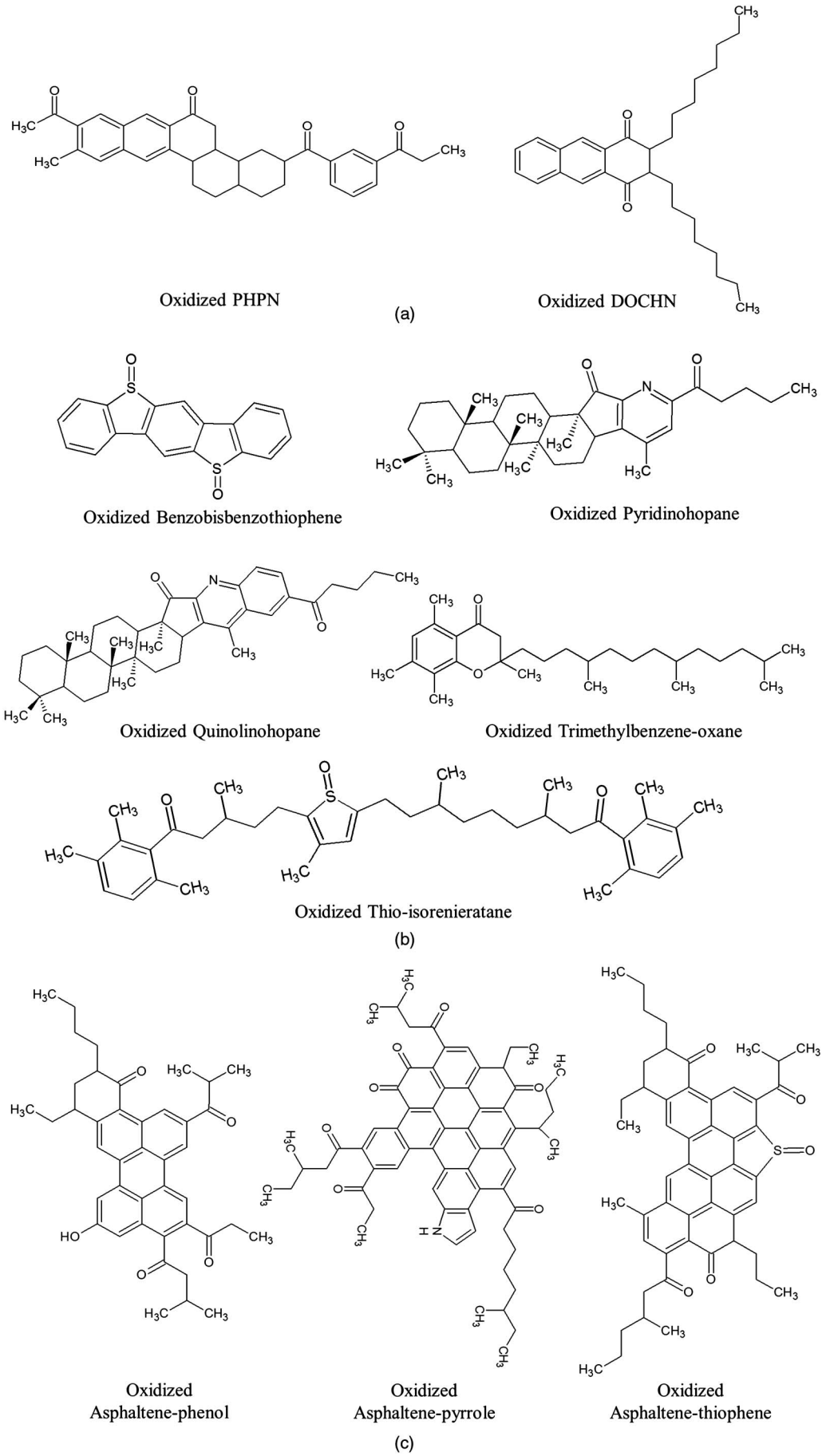

Fig. 4. Molecular structures in asphalt after oxidation: (a) oxidized aromatics; (b) oxidized resins; (c) oxidized asphaltenes

Table 1. Asphalt System Compositions before and after Oxidation

Asphalt fraction	Molecule	Number in AAA-1 model system	Percentage of each fraction before oxidation[a]	Percentage of each fraction after oxidation[a]	Experimental data before oxidation[b]
Saturates	Squalane	4	10.7	9.9	10.6
	Hopane	4			
Aromatics	PHPN	11	38.1	38.0	37.3
	DOCHN	13			
Resins	Quinolinohopane	4	30.6	31.1	31.8
	Pyridinohopane	4			
	Thioisorenieratane	4			
	Benzobisbenzothiophene	5			
	Trimethylbenzene-oxane	15			
Asphaltene	Asphaltene-pyrrole	2	16.5	16.9	16.2
	Asphaltene-phenol	3			
	Asphaltene-thiophene	3			

[a]Fraction percentage is standardized to match the experimental data (data from Li and Greenfield 2014b).
[b]Experimental data are from Jones's study (data from Jones 1993).

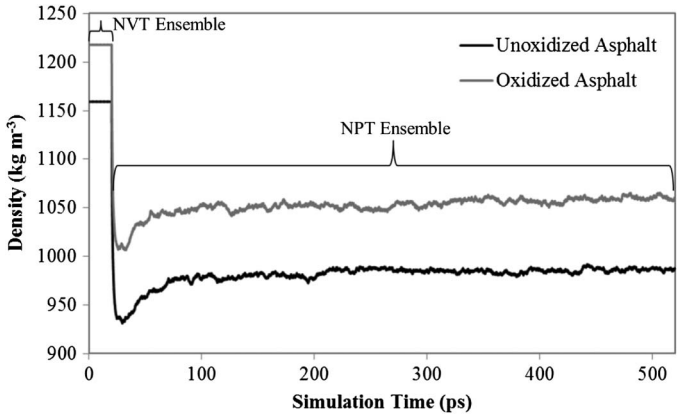

Fig. 5. Density simulation results of asphalt systems at 25°C

The simulation result of unoxidized asphalt system in this study is further compared with Li and Greenfield's (2014b) study regarding density changes at different temperatures as shown in Fig. 6. It can be seen that in both studies, the trends in the unoxidized asphalt's density changes at different temperatures are the same, demonstrating that the density of asphalt decreases with an increase in temperature. However, although the same unoxidized asphalt system was used in this study as Li and Greenfield's (2014a) proposal, the simulation results are not the same as those shown in Fig. 6. According to the linear fit results, the magnitude of slope for density versus temperature equation in Li and Greenfield's (2014b) study is higher than the one in this study. This indicates that the density of the modeled asphalt in Li and Greenfield's (2014a, b) study decreases more quickly with an increase in temperature than the density change observed in this study. Different simulation parameter might have caused the difference, or it could be attributable to the force field selections in the two studies.

The higher density of oxidized asphalt is caused by the enhanced aggregation process resulting from the nanoaggregation of the asphaltene fraction and decline in resin fraction and might be caused by hardening of asphalt after oxidation (Lemarchand et al. 2013; Pan and Tarefder 2016). Later in this study, this is investigated by the changes of isothermal compressibility and bulk modulus, which are used to interpret glass transition behavior change of asphalt caused by oxidation.

Isothermal Compressibility and Bulk Modulus

Isothermal compressibility, β_T, measures the volume change of a system based on the pressure changes at constant temperature. The bulk modulus, K, is the inverse of the isothermal compressibility and is used to measure the resistance of a material to uniform compression. These two physical quantities have been calculated by Tildesley and Allen (1987) as follows:

$$\beta_T = \frac{1}{K} = -V^{-1}\left(\frac{\partial V}{\partial P}\right)_T = \frac{1}{\langle V\rangle k_B T}(\langle V^2\rangle - \langle V^2\rangle) \qquad (1)$$

where k_B = Boltzmann constant; T = system temperature; V = system volume; and P = system pressure. The simulation parameter

Table 2. Number of Atoms in Unoxidized Asphalt System

Asphalt fraction	Molecule	Number of carbon atoms	Number of hydrogen atoms	Number of oxygen atoms	Number of nitrogen atoms	Number of sulfur atoms	Total number of atoms
Saturates	Hopane	35	62	0	0	0	97
	Squalane	30	62	0	0	0	92
Aromatics	DOCHN	30	46	0	0	0	76
	PHPN	35	44	0	0	0	79
Resins	Benzobisbenzothiophene	18	10	0	0	2	30
	Pyridinohopane	36	57	0	1	0	94
	Quinolinohopane	40	59	0	1	0	100
	Thioisorenieratane	40	60	0	0	1	101
	Trimethylbenzene-oxane	29	50	1	0	0	80
Asphaltenes	Asphaltene-pyrrole	66	81	0	1	0	148
	Asphaltene-phenol	42	54	1	0	0	97
	Asphatene-thiophene	51	62	0	0	1	114

Table 3. Number of Atoms in Oxidized Asphalt System

Asphalt fraction	Molecule	Number of carbon atoms	Number of hydrogen atoms	Number of oxygen atoms	Number of nitrogen atoms	Number of sulfur atoms	Total number of atoms
Saturates	Hopane	35	62	0	0	0	97
	Squalane	30	62	0	0	0	92
Aromatics	DOCHN	30	42	2	0	0	74
	PHPN	35	36	4	0	0	75
Resins	Benzobisbenzothiophene	18	10	2	0	2	32
	Pyridinohopane	36	53	2	1	0	92
	Quinolinohopane	40	55	2	1	0	98
	Thioisorenieratane	41	56	2	0	1	100
	Trimethylbenzene-oxane	29	48	2	0	0	79
Asphaltenes	Asphaltene-pyrrole	66	67	7	1	0	141
	Asphaltene-phenol	42	46	5	0	0	93
	Asphatene-thiophene	51	54	5	0	1	111

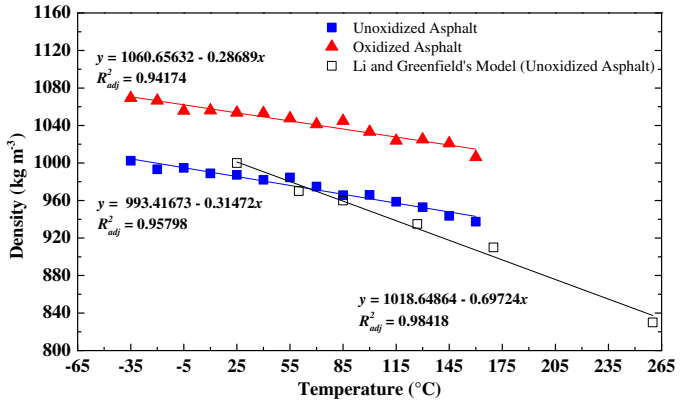

Fig. 6. Density changes of unoxidized and oxidized asphalt systems at different temperatures

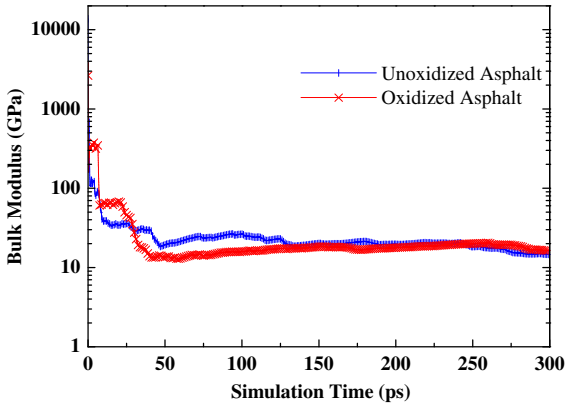

Fig. 7. Bulk modulus calculation result versus simulation time at −35°C

selections and procedures are the same as previously mentioned, and all the simulations reached equilibrium after 600,000 running steps in volume (after 400,000 running steps in the NPT ensemble with a simulation duration of 1 million running steps). For the last 600,000 simulation steps (300 ps), isothermal compressibility and bulk modulus for both unoxidized and oxidized asphalt systems were calculated. Larger temperature intervals were used for analysis to avoid errors and noise affecting the calculation results for a single temperature point. The volume fluctuations after equilibrium under −35, 40, 115, and 160°C (238.15, 313.15, 388.15, and 433.15 K) were selected for calculations.

All calculations were converged after 150 ps. One example of the bulk modulus calculation for unoxidized and oxidized asphalt systems under different simulation times at −35°C is shown in Fig. 7. Fig. 8 shows the average values of bulk modulus at the last 50 ps simulation duration for different temperatures, respectively. It is observed that the oxidized asphalt has lower isothermal compressibility and higher bulk modulus compared with unoxidized asphalt, which indicates that hardening happened after asphalt oxidation. Previous studies also showed an increase in elastic modulus of asphalt binder caused by oxidation (Allen et al. 2013; Tarefder and Faisal 2013). Moreover, the change trend of isothermal compressibility or bulk modulus at different temperatures is different between the unoxidized asphalt and oxidized asphalt, which indicates glass transition behavior change of the asphalt after oxidation. The isothermal compressibility of both unoxidized and oxidized asphalt systems increases with an increase in temperature, whereas bulk modulus shows the opposite trend.

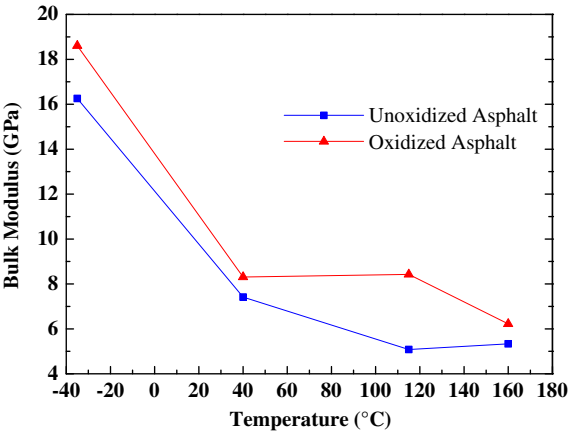

Fig. 8. Bulk modulus changes of asphalt before and after oxidation at different temperatures

Moisture Impacts on Asphalt before and after Oxidative Aging

Simulation Parameters

Water molecules were added to the asphalt simulation boxes before and after oxidation to analyze the impacts of moisture. Here, 1–10% moisture content by mass of the simulation boxes was considered

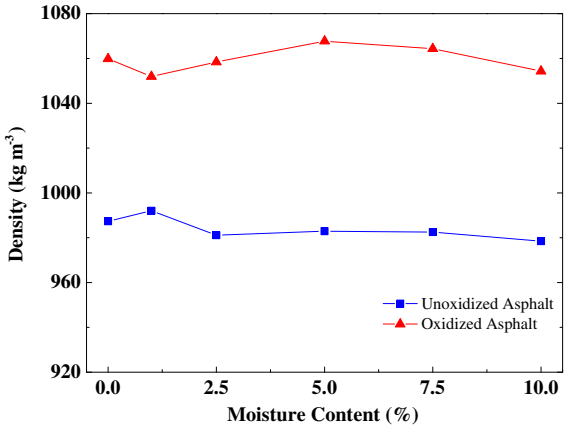

Fig. 9. Density changes of unoxidized and oxidized asphalts at different moisture contents

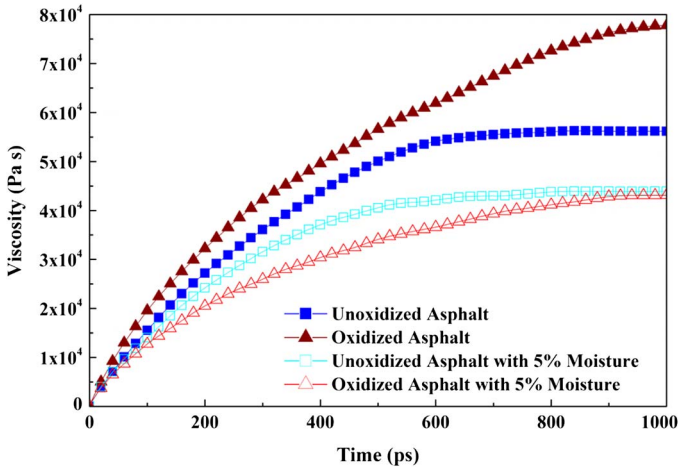

Fig. 10. Zero-shear viscosity calculation results of unoxidized and oxidized asphalts versus simulation time with and without moisture inclusion

with a content increment of 2.5%. Simulation temperature was set at room temperature (25°C). Simulation procedures were the same as the aforementioned density simulations. All simulations reached equilibrium. The MD simulations for zero-shear viscosity calculations for 0 and 5% moisture contents were conducted with a NPT ensemble after both unoxidized and oxidized asphalt systems reached density equilibrium. The simulations were conducted at a time step of 0.5 fs and run for 1 ns (2 million simulation steps).

Density Changes at Different Moisture Content

Fig. 9 shows the density changes of asphalt systems before and after oxidation at different moisture contents. It is observed that moisture content within 10% has an insignificant impact on the density change of the asphalt systems. For both unoxidized and oxidized asphalts, the density change from 0% moisture inclusion to 10% moisture inclusion is within 15 kg m^{-3}. However, the fluctuation of density is more significant for the oxidized asphalt at different moisture contents compared with that of the unoxidized asphalt. Generally, for both the unoxidized and oxidized asphalts, density initially increases with an increase in moisture content and starts decreasing at a certain moisture content. The maximum density is at 1% moisture content for the unoxidized asphalt, but at 5% moisture content for the oxidized asphalt. These indicate water has a greater effect on oxidized asphalt regarding density changes.

Zero-Shear Viscosity Changes under Different Moisture Content

The zero-shear viscosities of equilibrium asphalt systems were calculated by the Green-Kubo approach (Gordon 2003) as follows:

$$\eta = \frac{V}{k_B T}\int_0^\infty \langle P^s_{\alpha\beta}(0) P^s_{\alpha\beta}(t)\rangle dt \tag{2}$$

where k_B = Boltzmann constant; t = time; T = temperature; $P^s_{\alpha\beta}$ = instantaneous pressure tensor for off-diagonal element $\alpha\beta$; and V = system volume. To better improve convergence of the calculation, zero-shear viscosity was determined via averaging the three independent off-diagonal pressure tensors (Gordon 2003).

There is no ensemble restriction on using the Green-Kubo method for viscosity calculation according to the literature review and this study. Zhang and Ely (2004) used both NPT and NVT ensembles to predict the viscosity of alkane and alcohol systems by the Green-Kubo method and obtained good agreement with experimental results. Lee (2007) revisited the Green-Kubo formula to study the transport properties of liquid argon using both NPT and NVT ensembles and concluded that the difference in viscosity calculations under different ensembles was not significant. The same conclusion is also obtained by this study. Pan (2015) provided a comparison of off-diagonal pressure fluctuations under NPT and NVT ensembles.

The viscosity changes of the unoxidized and oxidized asphalt systems at 0 and 5% moisture contents over the simulation time are shown in Fig. 10. Without any moisture inclusion, the viscosity of unoxidized asphalt is considerably lower than that of the oxidized asphalt, which is approximately 2.2×10^4 Pa · s lower than that of the oxidized asphalt. This is consistent with Lemarchand et al.'s (2013) research on the chemical aging of the Cooee asphalt model, which concluded that an enhanced aggregation process after asphalt aging resulted in a viscosity increase. To prove the simulation duration lasted long enough to display stable values, standard deviations of zero-shear viscosity changes at the last 100,000 simulation steps were calculated for both unoxidized and oxidized asphalt systems with a value of 1.2 and 5.3, respectively (Pan and Tarefder 2016). The increase in viscosity with no moisture inclusion indicates that asphalt is harder after oxidation. However, after 5% moisture inclusion, it can be seen from Fig. 10 that the viscosity of unoxidized asphalt is higher than that of the oxidized asphalt, with a difference of 1.0×10^3 Pa · s. The standard deviations for the zero-shear viscosity changes in unoxidized and oxidized asphalt at the last 100,000 simulation steps are 5.4 and 2.7, respectively.

Fig. 11 further compares viscosities between asphalt systems with and without moisture inclusion. It can be seen that the zero-shear viscosities of both unoxidized and oxidized asphalt systems without moisture inclusion are much higher than those of the asphalt systems with moisture inclusion. Decreases in viscosity attributable to moisture inclusion has been shown by nanoindentation testing (Hossain 2013). Moreover, although oxidized asphalt tends to have a higher viscosity than unoxidized asphalt without moisture inclusion, the viscosity of oxidized asphalt decreases rapidly and finally becomes lower than that of unoxidized asphalt after 5% moisture inclusion. This indicates that oxidized asphalt is more susceptible to moisture regarding zero-shear viscosity changes. Pan (2015) explained in detail about zero-shear viscosity test using a dynamic shear rheometer (DSR).

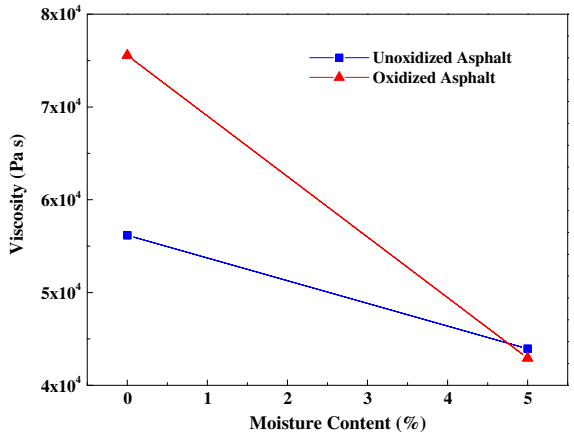

Fig. 11. Zero-shear viscosity changes of unoxidized and oxidized asphalts at different moisture contents

Conclusions

This study focused on how temperature and moisture impact unoxidized and oxidized asphalt properties using MD simulations of changes in density, isothermal compressibility, bulk modulus, and zero-shear viscosity. Conclusions are as follows:

- Asphalt density is temperature-dependent. The density of asphalt systems before and after oxidative aging decreases with an increase in temperature. Oxidized asphalt has a higher density than unoxidized asphalt but this decreases slightly more slowly than unoxidized asphalt. This might be caused by the hardening of asphalt after oxidation;
- Isothermal compressibility and bulk modulus are also very sensitive to temperature. Oxidized asphalt has a lower isothermal compressibility and higher bulk modulus than unoxidized asphalt at different temperatures. This proves that asphalt undegoes hardening after asphalt oxidation. The various change trends in isothermal compressibility and bulk modulus between unoxidized and oxidized asphalts at different temperatures indicates glass transition behavior changes after asphalt oxidation. In sum, the isothermal compressibility of asphalt systems before and after oxidative aging increases with an increase in temperature, whereas bulk modulus shows the opposite trend; and
- Moisture inclusion has greater adverse impacts on oxidized asphalt in terms of density and zero-shear viscosity changes. The changes in density values for asphalt systems before and after oxidative aging at different moisture contents are not significant. However, moisture causes more density fluctuations in oxidized asphalt. The zero-shear viscosities decrease with an increase in moisture inclusion for both asphalt systems. Moreover, the zero-shear viscosity of oxidized asphalt decreases more rapidly than that of unoxidized asphalt as a result of moisture inclusion.

Acknowledgments

The project was funded by the National Science Foundation (NSF) through the GOALI program; NSF Award No. 0900778.

Notation

The following symbols are used in this paper:

k_B = Boltzmann constant;
P = pressure;
$P^s\alpha\beta$ = instantaneous value of the off-diagonal pressure tensor element $\alpha\beta$;
t = time;
V = volume; and
η = zero-shear viscosity.

References

Al Halwachi, H. K., Yakovlev, D. S., and Boek, E. S. (2012). "Systematic optimization of asphaltene molecular structure and molecular weight using the quantitative molecular representation approach." *Energy Fuels*, 26(10), 6177–6185.

Allen, R. G., Little, D. N., Bhasin, A., and Lytton, R. L. (2013). "Identification of the composite relaxation modulus of asphalt binder using AFM nanoindentation." *J. Mater. Civ. Eng.*, 10.1061/(ASCE)MT.1943-5533.0000615, 530–539.

Chindaprasirt, P., Hatanaka, S., Mishima, N., Yuasa, Y., and Chareerat, T. (2009). "Effects of binder strength and aggregate size on the compressive strength and void ratio of porous concrete." *Int. J. Miner. Metall. Mater.*, 16(6), 714–719.

Corbett, L. W. (1969). "Composition of asphalt based on generic fractionation, using solvent deasphaltening, elution-adsorption chromatography, and densimetric characterization." *Anal. Chem.*, 41(4), 576–579.

Corbett, L. W., and Merz, R. E. (1975). "Asphalt binder hardening in the Michigan test road after 18 years of service." *Transp. Res. Rec.*, 544, 27–34.

Fraaije, J. H. G., et al. (2014). *Culgi manual 8.0*, Culgi, Leiden, Netherlands.

Gordon, P. (2003). "Influence of simulation details on thermodynamic and transport properties in molecular dynamics of fully flexible molecular models." *Mol. Simul.*, 29(8), 479–487.

Greenfield, M. L. (2011). "Molecular modelling and simulation of asphaltenes and bituminous materials." *Int. J. Pavement Eng.*, 12(4), 325–341.

Greenfield, M. L., and Zhang, L. (2009). "Developing model asphalt systems using molecular simulation." *Final Rep.*, URITC, Kingston, RI.

Hansen, J. S., Lemarchand, C. A., Nielsen, E., Dyre, J. C., and Schrøder, T. (2013). "Four-component united-atom model of bitumen." *J. Chem. Phys.*, 138(9), 094508–094513.

Hossain, M. I. (2013). "Modeling moisture-induced damage in asphalt concrete." Ph.D. dissertation, Dept. of Civil Engineering, Univ. of New Mexico, Albuquerque, NM.

Jones, D. R. (1993). *Asphalt cements: A concise data compilation*, Vol. 1, Strategic Highway Research Program, National Research Council, Washington, DC.

Lee, S. H. (2007). "Molecular dynamics simulation study of the transport properties of liquid argon: The Green-Kubo formula revisited." *Bull. Korean Chem. Soc.*, 28(8), 1371–1374.

Lemarchand, C. A., Bailey, N. P., Todd, B. D., Daivis, P. J., and Hansen, J. S. (2015). "Non-Newtonian behavior and molecular structure of Cooee bitumen under shear flow: A non-equilibrium molecular dynamics study." *J. Chem. Phys.*, 142(24), 244501.

Lemarchand, C. A., Schrøder, T. B., Dyre, J. C., and Hansen, J. S. (2013). "Cooee bitumen: Chemical aging." *J. Chem. Phys.*, 139(12), 124506.

Lemarchand, C. A., Schrøder, T. B., Dyre, J. C., and Hansen, J. S. (2014). "Cooee bitumen. II: Stability of linear asphaltene nanoaggregates." *J. Chem. Phys.*, 141(14), 144308.

Lesueur, D. (2009). "The colloidal structure of bitumen: Consequences on the rheology and on the mechanisms of bitumen modification." *Adv. Colloid Interface Sci.*, 145(1–2), 42–82.

Li, D. D., and Greenfield, M. L. (2014a). "Chemical compositions of improved model asphalt systems for molecular simulations." *Fuel*, 115, 347–356.

Li, D. D., and Greenfield, M. L. (2014b). "Viscosity, relaxation time, and dynamics within a model asphalt of larger molecules." *J. Chem. Phys.*, 140(3), 034507.

Lu, Y., and Wang, L. (2010). "Nanoscale modelling of mechanical properties of asphalt-aggregate interface under tensile loading." *Int. J. Pavement Eng.*, 11(5), 393–401.

Ma, T., Huang, X., Mahmoud, E., and Garibaldy, E. (2011). "Effect of moisture on the aging behavior of asphalt binder." *Int. J. Miner. Metall. Mater.*, 18(4), 460–466.
Mannan, U. A., Islam, M. R., Weldegiorgis, M., and Tarefder, R. A. (2015). "Experimental investigation on rheological properties of recycled asphalt pavement mastics." *Appl. Rheol.*, 25(22753), 1–9.
Martín-Martínez, F. J., Fini, E. H., and Buehler, M. J. (2015). "Molecular asphaltene models based on Clar sextet theory." *RSC Adv.*, 5(1), 753–759.
Mayo, S. L., Olafson, B. D., and Goddard, W. A., III. (1990). "DREIDING: A generic force field for molecular simulations." *J. Chem. Phys.*, 94(26), 8897–8909.
MOPAC 2012 [Computer software]. Stewart Computational Chemistry, Colorado Springs, CO.
Pan, J. (2015). "A study of asphalt aging behavior using molecular dynamics simulation." Ph.D. dissertation, Dept. of Civil Engineering, Univ. of New Mexico, Albuquerque, NM.
Pan, J., and Tarefder, R. A. (2016). "Investigation of asphalt aging behaviour due to oxidation using molecular dynamics simulation." *Mol. Simul.*, 42(8), 1–12.
Pan, T., Lu, Y., and Lloyd, S. (2012). "Quantum-chemistry study of asphalt oxidative aging: An XPS-aided analysis." *Ind. Eng. Chem. Res.*, 51(23), 7957–7966.
Petersen, J. C. (1984). "Chemical composition of asphalt as related to asphalt durability: State of the art." *Transp. Res. Rec.*, 999, 13–30.
Petersen, J. C. (2009). "A review of the fundamentals of asphalt oxidation: Chemical, physicochemical, physical property, and durability relationships." *Transportation Research Circular No. E-C140*, Transportation Research Board, Washington, DC.
Petersen, J. C., and Glaser, R. (2011). "Asphalt oxidation mechanisms and the role of oxidation products on age hardening revisited." *Road Mater. Pavement Des.*, 12(4), 795–819.
Tarefder, R., and Faisal, H. (2013). "Nanoindentation characterization of asphalt concrete aging." *J. Nanomech. Micromech.*, 10.1061/(ASCE)NM.2153-5477.0000061, 1–8.
Tarefder, R. A., and Arisa, I. (2011). "Molecular dynamic simulations for determining change in thermodynamic properties of asphaltene and resin because of aging." *Energy Fuels*, 25(5), 2211–2222.
Tildesley, D. J., and Allen, M. P. (1987). *Computer simulation of liquids*, Clarendon, Oxford, U.K.
Zhang, H., and Ely, J. F. (2004). "AUA model NEMD and EMD simulations of the shear viscosity of alkane and alcohol systems." *Fluid Phase Equilib.*, 217(1), 111–118.
Zhang, L., and Greenfield, M. L. (2007a). "Molecular orientation in model asphalts using molecular simulation." *Energy Fuels*, 21(2), 1102–1111.
Zhang, L., and Greenfield, M. L. (2007b). "Relaxation time, diffusion, and viscosity analysis of model asphalt systems using molecular simulation." *J. Chem. Phys.*, 127(19), 194502.
Zhang, L., and Greenfield, M. L. (2008). "Effects of polymer modification on properties and microstructure of model asphalt systems." *Energy Fuels*, 22(5), 3363–3375.
Zhang, L., and Greenfield, M. L. (2010). "Rotational relaxation times of individual compounds within simulations of molecular asphalt models." *J. Chem. Phys.*, 132(18), 184502.